Evidence for Poole–Frenkel conduction in individual SiC nanowires by field emission transport measurements

M. Choueib,[a] A. Ayari, P. Vincent, S. Perisanu, and S. T. Purcell[b]
Université de Lyon, F-69000, France, Université Lyon 1, Laboratoire PMCN, CNRS, UMR 5586, F69622 Villeurbanne Cedex, France.

(Received 18 October 2010; accepted 14 December 2010; published online 5 April 2011)

In this paper we examine carrier transport mechanisms in individual Silicon Carbide nanowires (NWs) by an original use of field emission (FE). Total energy distributions were measured as a function of temperature and extraction voltage allowing us to determine the voltage drops along the NWs and thus the temperature-dependent current-voltage $(I-V-T)$ characteristics. The measurements were analyzed using different transport mechanisms of which only the Poole–Frenkel model gives an excellent fit. The dielectric constant was estimated for several samples at $\varepsilon \sim 10$ in excellent agreement with the bulk value. The characteristic trap energies, E_a, were determined from the $I-V-T$ data to be ~0.3 eV. In general this work shows how FE can be used for transport measurements on individual semiconducting NWs. © *2011 American Institute of Physics*.
[doi:10.1063/1.3556736]

I. INTRODUCTION

Semiconducting one-dimensional (1D) objects such as nanowires (NWs) are currently being intensively studied as a result of their importance in fundamental research and for their potential in the fabrication of nanoscale electronic, optoelectronic, and sensor devices.[1] One recurring theme in this subject is that the essential characterization and control of transport phenomenon on such small samples is arduous, to the point that the doping level is often left undetermined. This problem is becoming even more visible because researchers from different horizons are currently exploring a wide variety of top-down and bottom-up fabrication techniques to produce samples with different degrees of structural perfection, surface treatments, and physical entanglement. Certain approaches have been successfully adopted, including the integration of NWs with specialized surfaces into transistor devices[2] and advanced microscopy techniques,[3–5] but the use of such methods is far from routine. As explained next, we are exploring an original use of field emission (FE) for the characterization of semiconducting NWs as well as for their potential as electron sources.

Electron field emission is generally used for studying fundamental surface physics at a tip apex (crystal structure, work function, tunneling, field enhancement factor, etc.) or as the basis of a class of electron cathodes. We have been following a different tack by using FE to simultaneously probe different physical aspects of individual carbon nanotubes (CNTs) such as electrical resistance, thermal conductivity, and optical and mechanical properties.[6] FE energy spectroscopy (FEES) that measures the total energy distributions (TEDs) of the emitted electrons is a particularly useful tool in this effort. More recently, we have been extending these techniques to semiconducting NWs. In comparison with CNTs there has been much less work on FE from semiconducting NWs even though their band gaps give novel possibilities not open to metallic CNTs used in all FE experiments to date. In principle, FE from semiconductors is more complicated than from metals because the low carrier concentration can allow penetration of the external electric field into the semiconductor and band bending to considerable depths. This can result in strong and interesting saturation effects in the emitted current.[7,8] Among the numerous studies on semiconductor field emitters there are only a few that show these saturation effects, and those are for standard emitter tips fabricated from bulk samples.[8–10] Such effects have only recently been observed for semiconducting NWs by our group.[11] This is because of the difficulty of preparing samples of sufficient quality that avoids artifacts such as unwanted surface currents, which tend to cause semiconducting emitters to behave similar to metals and to lead to problems in reproducibility.[12] In situ surface cleaning by heat treatments and low-energy ion bombardment proved to be necessary.

We have extensively studied the mechanical properties of wide bandgap (2.4 eV) SiC NWs[13–15] and have also identified the doping type by FE.[11] However the first analysis[11] needs to be extended in order to fully explain the differences between these results, the theory,[7] and experiments on bulk semiconductor samples[8–10] and thus to better understand the transport in these samples. In this paper, we present more consistent data from FE studies on individual SiC NWs and accompanying analysis that shows that the electronic transport is well described by the Poole–Frenkel (PF) model.

The article is organized as follows: the experimental procedure for sample preparation and FE measurements are presented in section II, the results are given in section III, and section IV is dedicated to discussion. Conclusions are finally drawn in section V.

II. EXPERIMENTAL

Cubic 3C-SiC NWs were synthesized by a pure vapor solid process without catalyst.[16] The patented technique[17]

[a]Electronic mail: may_choueib@hotmail.com.
[b]Electronic mail: stephen.purcell@lpmcn.univ-lyon1.fr.

produces large quantities of very pure samples interesting for industrial applications particularly in composites. A characterization of their transport properties may open other applications and presents a first testing ground for our field emission techniques. Fifteen samples of individual SiC NWs of different diameters ($30 \rightarrow 250$ nm) and lengths were extensively studied by FE. The NWs were attached to tungsten tips fixed on heating loops allowing sample cleaning and temperature-dependent FE studies. Figure 1 shows a scanning electron microscopy image of two measured NWs denoted NW1 (diameter $\Phi = 250$ nm, length $L = 55$ μm) and NW2 ($\Phi = 30$ nm, $L = 2.5$ μm). Earlier reported transmission electron microscopy observations showed crystalline samples with alternating sections of near perfect monocrystals and sections with a high density of stacking faults.[16] A very short mean free path for electron transport can be anticipated for the later. FE measurements were performed in an ultrahigh vacuum system at a pressure 2×10^{-10} Torr. The experimental setup for the FE measurements and details of measurement procedures have been reported previously.[11] In brief, FE currents, I, were measured as a function of the total negative voltage V_A, and over a wide range of temperatures. Our installation has the great advantage of having a hemispherical energy analyzer which allows a direct measurement of the TEDs of the emitted electrons. As previously reported,[6,11] the TEDs gives the Fermi level E_F at the NW apex and thus the voltage drop V across the NW. Plotting I against V is similar to a two-point transport measurement with, however, only one bias direction available (see Fig. 2). These experiments allowed systematic $I-V-T$ measurements in single NWs as detailed in the next section.

III. RESULTS

FE current measurements are usually displayed in Fowler–Nordheim (FN) plots, i.e. $\log(I/V_A^2)$ versus $1/V_A$. Our previous studies on FE from SiC NWs[11] revealed a strong nonlinearity in the FN plots predicted by the theory of FE from semiconductors as shown in Fig. 3. In this figure, we present FN curves of the experimental data for NW1 with increasing temperature. Three distinct regions can be distinguished: At the low current, Region I ($< 10^{-13}A$) follows a standard linear FN plot as for emission from metals. The lowest currents were measured with a single electron counter. In the medium range, Region II, the current increases much more slowly with V_A, or "saturates." This saturation is due to insufficient carrier supply by thermal excitation across the gap. It results in a large depletion zone starting at the apex, associated field penetration into the semiconductor, and strong band bending. I is strongly dependent on temperature and light because these generate extra free carriers. Light-induced effects will be presented in a future publication. Finally, one notices the beginning of a Region III at the highest tested currents, which appears again to give metal-like FN plots. The rapid increase in III occurs because the field is sufficient for impact ionization in the depletion zone. The slopes of the $I-V$ curves measured here for the saturation regime are actually quite large in comparison to the theory. We have reported previously[11] that varying slopes can be attributed to additional transport mechanisms assured by energy-trap levels E_A in the bandgap in the depletion region. Supported by the field dependence of E_A and referring to others' work,[10] the transport mechanism was suggested to be the Poole–Frenkel effect,[18] although an in-depth analysis was lacking. In order to investigate the transport mechanism correctly, more extensive measurements of the TEDs are presented here to determine the voltage drops in NWs along with a fuller analysis. The measured voltage drops along the emitter can reached several hundreds of volts. An $I-V-T$ series for a SiC NW is plotted in Fig. 4(a). These plots are clearly nonlinear and the nonlinearity

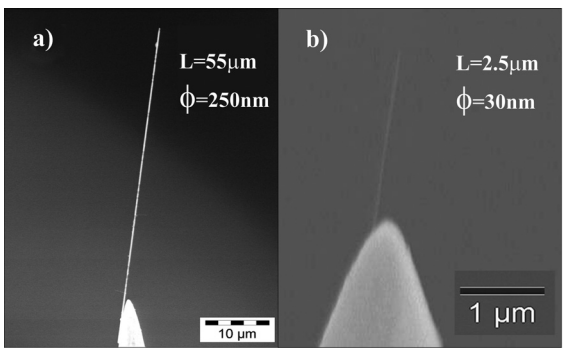

FIG. 1. SEM images of two SiC nanowires attached to tungsten tips, denoted (a) NW1 of diameter $\Phi = 250$ nm and length $L = 55$ μm and (b) NW2 of $\Phi = 30$ nm and $L = 2.5$ μm.

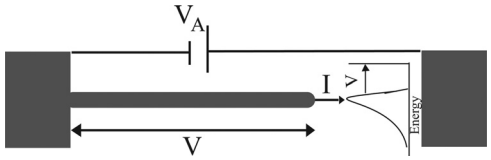

FIG. 2. Schematic illustration of the equivalent to a two-point measurement of our measurement: The position of the TED peak measured by energy analyzer gives the voltage drop along the nanowire.

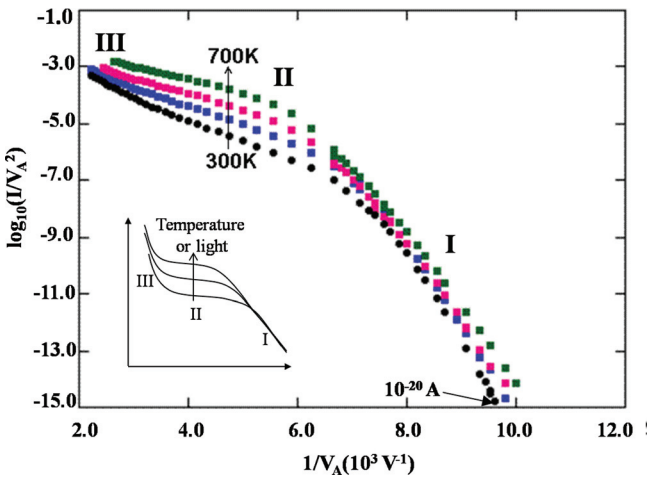

FIG. 3. (Color online) Fowler–Nordheim plots for NW1 with increasing temperature. In this curve, we distinguish the three regions predicted for field emission from semiconductors: region I standard Fowler–Nordheim as in metal, region II saturation of current limited by insufficient carrier supply that involves depletion zone, region III impact ionization at high electric field in depletion zone. Inset: Fowler–Nordheim plot expected for samples approaching the ideal case of p-type doping.

becomes less pronounced at high temperature. This means that with increasing temperature the carrier concentration increase was able to provide a sufficient supply of electrons to the FE region, and region I extends to a higher V_A. Thus at high temperature the FN plots correspond mostly to region I, i.e., standard FN emission (Fig. 3). At low temperature weak carrier concentration enhances the saturation and nonlinear $I-V$ curves. The same curves are presented in a semilog plot in Fig. 4(b) for comparison with the current-voltage characteristics of a pn junction in reverse bias (see inset) for which the physics is similar.[8] One notices that the measured curves have a rather weak saturation in comparison, as a result of the specific transport mechanism. The mechanism of conduction in region II is discussed next.

IV. DISCUSSION

The nonlinear $I-V$ characteristics may be due to hopping or other trap-mediated types of transport or due to a Schottky barrier at the contact between the W support tip and the SiC NW. Simple poor contact effects can be excluded since the measurements give similar results for different nanowires and it is unlikely that they can support hundreds of Volts. Four different possible transport mechanisms were considered to explain the nonlinearity: Schottky barrier (SB), Poole–Frenkel (PF), space-charge limited conduction (SCL), and variable range hopping (VRH). For SB and PF models, conduction may by controlled at the metal–semiconductor interface with a depletion region at the contact. The theory of FE from p-type doped semiconductors predicts the electric field and depletion region to be strongest near the FE end. The conduction may also be controlled by PF, SCL, and VRH near the FE end of the NW where carriers move or hop respectively between the traps for the SCL and VRH mechanisms. The models can be summed up as follows:

- For transport via a SB at the metal–semiconductor contact, the $I-V$ characteristics at constant temperature T follow:[19]

$$I \sim \left[\exp\left(\frac{qV}{k_B T}\right) - 1\right] \tag{1}$$

where q is the electronic charge and k_B is Boltzmann's constant.

- PF transport is characterized by thermal excitation of carriers trapped within a potential well into the conduction band and is enhanced by electric field. The barrier height is the depth of the trap potential inside the bandgap. Conduction via the PF mechanism is described by:[18]

$$I \sim V \exp\left(\frac{\beta_{PF}\sqrt{V} - \phi_{PF}}{k_B T}\right) \tag{2}$$

where ϕ_{PF} is the barrier height of the trap potential and β_{PF} is the barrier lowering which will be discussed in more detail subsequently.

- In a simple hopping model, charge may hop between adjacent sites as a result of an external electric field. The expression of the current within the hopping model is given by:[20]

$$I \sim \sinh\left(\frac{AV}{k_B T}\right) \tag{3}$$

where A is a constant that depends on the hopping distance and the length of the sample.

- SCL conduction can occur when the injected charge is so high that it leads to a current reduction due to Coulomb interaction. The transport then occurs by carriers moving between traps. The $I-V$ characteristics for SCL with a single trap energy[21] follow:

$$I \sim V^2. \tag{4}$$

However, samples such as these SiC NWs with different defects and structural imperfections will have a range of trap energies.[22] In this case, $I-V$ characteristics for SCL are given by:

$$I \sim V^{l+1} \tag{5}$$

where $l = T_t/T$ and T_t is called the trap temperature.

Each of these mechanisms were evaluated by comparing the measured $I-V$ curves with curve fits to the different models. Figure 5 presents the results of fits to the experimental data presented in Fig. 4 at room temperature. The solid line is a fit to the data using the PF expression as given by Eq. (2). The long-dash, short-dash, and dotted lines are fits with the SB, SCL, and VRH models, respectively, as given

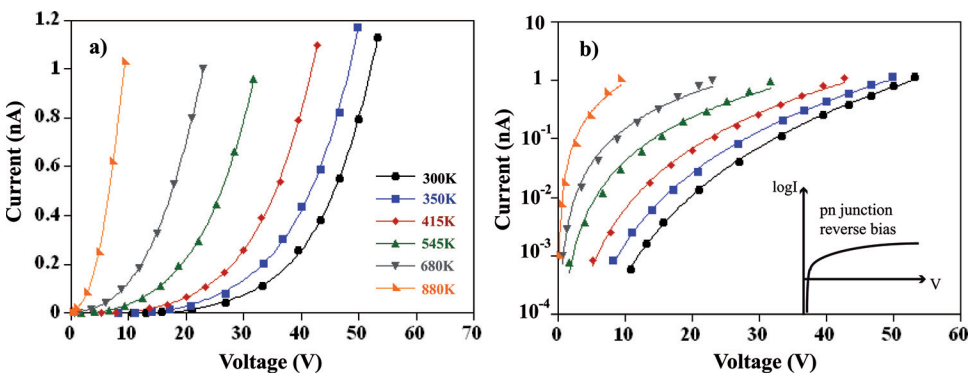

FIG. 4. (Color online) (a) Emission current versus tip voltage drop for NW2 at different temperatures. The nonlinearity of the curves becomes less pronounced at high temperature. (b) The same curves in semilog plot for comparison with the current-voltage characteristics for pn junction in reverse bias (inset).

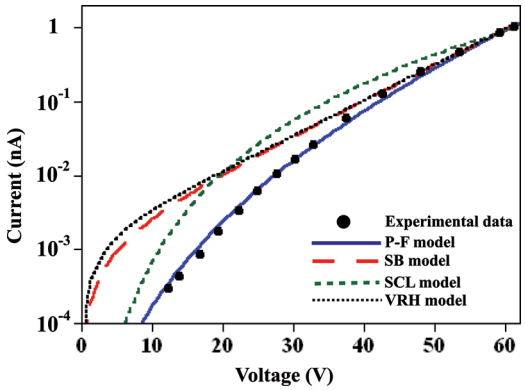

FIG. 5. (Color online) Current-voltage characteristics of NW2 in the saturation region II at room temperature and fits with different models to determine the conduction mechanism. The long-dashed line, short-dashed line, and the dotted line are fits with Schottky barrier, space charge limited conduction, and variable range hopping models, respectively. The solid line is a fit obtained within the Poole–Frenkel model and gives the best fit to the experimental data.

by Eqs. (1), (5) ($l=3$), and (3). It is clear that the PF model gives by far the best fit to the experimental results at room temperature.

$I-V$ curves for a system exhibiting PF conduction should scale as $\log(I/V)$ versus $V^{1/2}$. This plot will yield a straight line where the slope is proportional to β_{PF}. From Eq. (2), we can express this slope as:

$$S=\frac{\beta_{PF}}{k_B T} \tag{6}$$

and β_{PF} is a coefficient related to dielectric constant of the material ε by:

$$\beta_{PF}=\sqrt{\frac{q^3}{d\pi\varepsilon_0\varepsilon}} \tag{7}$$

where ε_0 is the permittivity of free space and d is the sample's length. So the slope of such a plot is a constant dependent on ε and T and can be used as a further verification that conduction is due to the PF mechanism. In Fig. 6, we present linear PF plots for NW1 [Fig. 1(a)] and NW3 ($\Phi=100$ nm, $L=5$ μm). β_{PF} determined from the fits of PF plots for the relatively shorter NWs gave a dielectric constant in excellent agreement with the dielectric constant of bulk SiC (for 3C-SiC, $\varepsilon_{bulk}=9.72$).[23] For example, we obtained $\varepsilon=9.9$ for NW2 [Fig. 1(b)], and $\varepsilon=10.05$ for NW3. However $\varepsilon=4.1$ was found for NW1 with $L=55\mu$m which is less than half that of bulk SiC. In fact, the calculation assumed that the voltage drop occurs over the full length of the NWs [$d=L$ in Eq. (7)]. We have already mentioned that the electric field penetrates into the NWs with the formation of a depletion region. For very long emitters the majority of the voltage drop would occur toward the FE end of the NWs. In this case the electric field is determined by evaluating the voltage drop across the depletion region instead of the full NWs length. It is difficult to estimate the size of the depletion region because of the complexity of the material and uncertainty of the conduction mechanism of these NWs.[11] However, this region can be very broad, as has been demonstrated theoretically[7] and experimentally[8] and this is supported by the excellent value of ε obtained for the NWs of up to 10 μm in length. This means that assuming $d=L$ in Eq. (7) is correct for $L<10$ μm. From another point of view one can estimate the length of the depletion zone. For NW1, considering $\varepsilon=9.8$, one gets from Eq. (7) a depletion zone of $d=23$ μm which explains why the 55 μm NW2 gives such a large error in ε.

A. Temperature dependence

Up to this point we have discussed only the room temperature data. Typical $I-V-T$ characteristics on NW2 for $T=300$–880 K are shown in Figs. 4 and 7. The corresponding PF curves and fits are presented in Fig. 7(a). The plots are quite linear and consistent with the PF conduction model. The slopes decrease with increasing T, except for the last curve. As already mentioned the length of the depletion zone d can be estimated from these slopes [Eqs. (6) and (7)]. Figure 7(b) shows that the fitted d decreases with T. This is expected because the number of free carriers increases strongly with temperature while the collisions are still controlled by the high defect density. This decreases the penetration of the field into the NWs.

$I-V-T$ measurements for region II give the thermal activation energies E_a. For several NWs, we showed that E_a decreases with increasing voltage in agreement with the PF model and was estimated to be ~ 0.3 eV. This value does not correspond to known dopant levels in SiC[23] but is a reasonable trap energy.

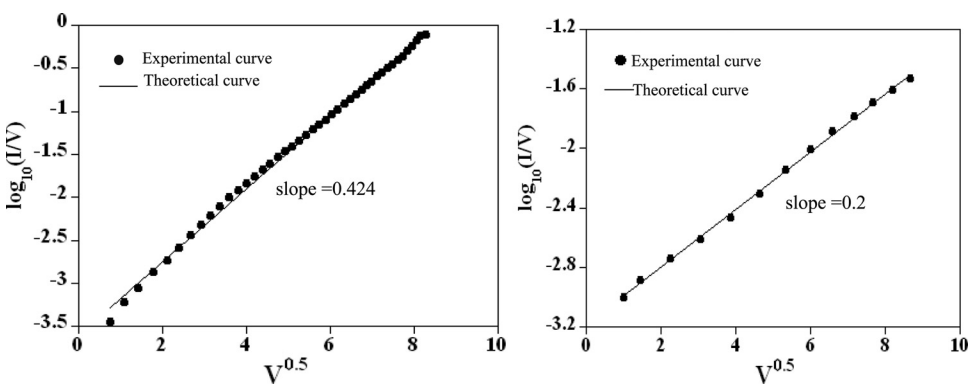

FIG. 6. Poole–Frenkel plots for two nanowires: on the right NW1 ($\Phi=250$ nm and length $L=55\mu$m) and on the left NW3 ($\Phi=100$ nm and length $L=5\mu$m). These curves are linear and consistent with the Poole–Frenkel conduction model. The best fit line (solid) to the Poole–Frenkel plot is also included.

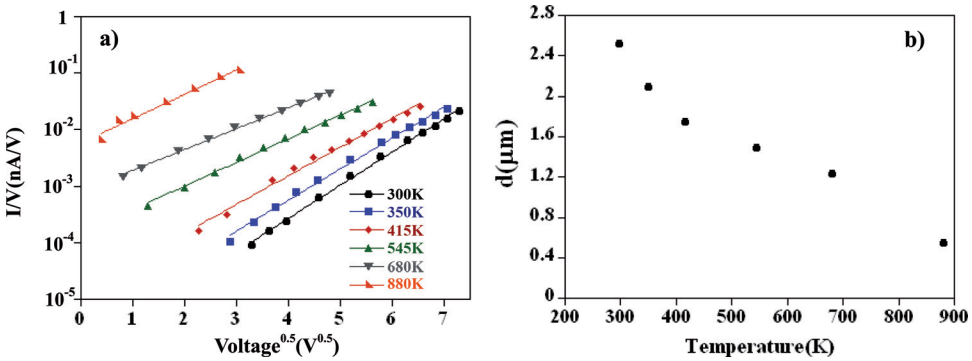

FIG. 7. (Color online) (a) Temperature-dependent $I-V$ plots with curve fits using expressions for Poole–Frenkel transport for NW2. At the highest temperature (880 K) and low field that corresponds to the Fowler–Nordheim region I, the data deviates from the Poole–Frenkel model. (b) The calculated d from Eq. (7) decreases with increasing temperature. One notices the deviation of the last point at 880 K.

V. CONCLUSION

The main conclusion of the analysis above is that the FE $I-V-T$ data measured using an energy analyzer can be used to understand the transport mechanism in semiconducting NWs. The measured nonlinear $I-V-T$ curves were fitted with various models to determine whether the transport mechanism was by Schottky barrier, space charge limited conduction, hopping, or Poole–Frenkel conduction. This last model gives a best fit to experimental data for our less-than-perfect SiC NWs. The fits give a dielectric constant $\varepsilon \sim 10$ for several samples, in good agreement with the bulk value, which strongly reinforces the validity of the analysis. The Poole–Frenkel model was used to estimate the size of the depletion zone, which decreases with temperature. The thermal activation of trap energies could be estimated from the $I-V$ data to be ~ 0.3 eV.

Such a use of FE is original and needs to be tested on more ideal samples with long mean free paths and transport controlled by standard doping. The measurements and theory can then provide a clear comparison with these results. This will provide further impetus to extend the FE analysis of nanowires into the optical and time domains. We are now carrying out experiments on much more ideal Si nanowire samples for which the preliminary results are highly encouraging.

ACKNOWLEDGMENTS

This work was carried out within the framework of the "Plateforme nanofils et nanotube Lyonnaise de l'Université Lyon 1." The authors acknowledge M. Bechelany and D. Cornu for the SiC nanowires.

[1]C. Lieber, MRS Bull. **32**, 99 (2007)
[2]W. Lu, P. Xie, and C.M. Lieber, IEEE Trans. Electron Devices **55**, 2859 (2008).
[3]S. Hoffmann, J. Bauer, C. Ronning, Th. Stelzner, J. Michler, C. Ballif, V. Sivakov, and S. H. Christiansen, Nano Lett. **9**,1341 (2009)
[4]M. I. den Hertog, H. Schmid, D. Cooper, J. L. Rouviere, M. T. Bjork, H. Riel, P. Rivallin, S. Karg, and W. Riess, Nano Lett. **9**, 3837 (2009).
[5]J. E. Allen, D. E. Perea, E. R. Hemesath and L. J. Lauhon, Adv. Mater. **21**, 3067 (2009)
[6]S. T. Purcell, P. Vincent, M. Rodriguez, C. Journet, S. Vignoli, D. Guillot, and A. Ayari, Chem. Vap. Deposition **12**, 331 (2006).
[7]L. M. Baskin, O. I. Lvov, and G. N. Fursey, Phys. Status Solidi B **47**, 49 (1971)
[8]J. R. Arthur, J. Appl. Phys. **36**, 3221 (1965).
[9]D. K. Schroder, R. N. Thomas, J. Vine, and H. C. Nathanson, IEEE Trans. Electron Devices **21**,785 (1974).
[10]K. X. Liu, C. J. Chiang, and J. P. Heritage, J. Appl. Phys. **99**, 034502 (29 June 2006).
[11]M. Choueib, A. Ayari, P. Vincent, M. Bechelany, D. Cornu, and S. T. Purcell, Phys. Rev. B. **79**, 075421 (2009).
[12]G. Fursey, Appl. Surf. Sci. **94/95**, 44 (1996)
[13]A. Ayari, P. Vincent, S. Perisanu, M. Choueib, V. Gouttenoire, M. Bechelany, D. Cornu, and S. T. Purcell, Nano Lett. **7**, 2252 (2007).
[14]P. Vincent, S. Perisanu, A. Ayari, M. Choueib, V. Gouttenoire, M. Bechelany, D. Cornu, and S. T. Purcell, Phys. Rev. B **76**, 085435 (2007).
[15]S Perisanu, V. Gouttenoire, P. Vincent, A. Ayari, M. Choueib, M. Bechelany, D. Cornu, and S. T. Purcell, Phys. Rev. B **77**, 165434 (2008).
[16]M. Bechelany, A. Brioude, P. Stadelmann, G. Ferro, D. Cornu, and P. Miele, Adv. Funct. Mater. **17**, 3251 (2007).
[17]M. Bechelany, D. Cornu, P. Miele, International patent WO 2006/067308 (29 June 2006).
[18]J. R. Yeargan and H.L. Taylor, J. Appl. Phys. **39**, 5600 (1968).
[19]S. M. Sze, *Physics of Semiconductor Devices* (Wiley, Hoboken, NJ, 1981).
[20]N. F. Mott and E.A. Davis, *Electronic Processes in Non-Crystalline Materials* (Clarendon, Oxford, 1979).
[21]A. Rose, Phys Rev. **97**, 1538 (1955)
[22]M.A. Lampert, and P. Mark, *Current Injections in Solids* (Academic Press, New York, 1970).
[23]G. L. Harris, *Properties of Silicon Carbide* (INSPEC, London, UK, 1995).